ACS APPLIED MATERIALS & INTERFACES

Research Article

www.acsami.org

Self-Healing of Core–Shell Magnetic Polystyrene Nanocomposites

Mitra Yoonessi,*[,†] Bradley A. Lerch,[§] John A. Peck,[‡] Richard B. Rogers,[§] Francisco J. Solá-Lopez,[§] and Michael A. Meador[§]

[†]Ohio Aerospace Institute, Cleveland, Ohio 44135, United States

[§]NASA Glenn Research Center, Cleveland, Ohio 44135, United States

[‡]Department of Geosciences, University of Akron, Akron, Ohio 44325, United States

Supporting Information

ABSTRACT: High heat generation is reported in core–shell magnetic nanoparticle polystyrene (PS) nanocomposites (3.5, 10 wt %) when they are placed in a high-frequency ac magnetic field. These magnetic nanoparticles with cobalt iron oxide core and manganese iron oxide shell were synthesized and characterized by wide-angle X-ray scattering (WAX), thermal gravimetric analysis (TGA), transmission electron microscopy (TEM), and ac field gradient magnetometery. When placed in a high-frequency ac magnetic field, the thermal energy generated in the magnetic polystyrene nanocomposites resulted in a surface temperature increase. The heat generation is attributed to the contribution of Néel relaxation and hysteresis of the core–shell magnetic nanoparticles in the solid state. The maximum surface temperature increased with increasing nanoparticle content and resulted in melting of the magnetic polystyrene nanocomposite.

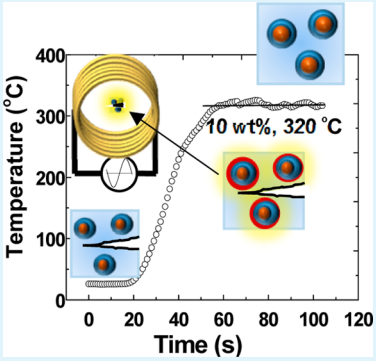

KEYWORDS: *magnetic polymer nanocomposite, magnetic nanoparticles, self-healing, smart polymers, polystyrene*

1. INTRODUCTION

Magnetic nanoparticle polymer nanocomposites are an important class of polymeric materials with applications such as bioseparation,[1] magnetic sensors,[2] optoelectronic storage,[3] miniaturized antenna,[4] shape memory polymers and polymer actuators,[5,6] and EMI shielding.[7−9] Magnetic nanoparticles have extraordinary properties depending on their chemical composition, size, shape, and aspect ratio.[10] Surface functionalization of magnetic nanoparticles is essential for targeted design performance in many applications such as hyperthermia, drug delivery, magnetic resonance imaging (MRI), biocompatible cell labeling, and more.[1−9] Functionalization could be tailored using biocompatible ligands targeted for cell internalized and in vivo monitoring, or chemical functionality for dispersion in a polymeric system. Magnetic nanoparticles have been used for recording media, magnetic resonance imaging, targeted drug delivery, and hyperthermia.[11−15] Magnetic nanoparticles can be tailored for specific target tumor location and to generate heat for cancer treatments.[15]

The magnetic characteristics of magnetic nanoparticles depend on their size, aspect ratio, and chemical composition.[10] Heat generation in ac magnetic field is determined by specific loss power (SLP). Characteristics of magnetic nanoparticles which contribute to the specific loss power (SLP) are the magnetic nanoparticle diameter (D), magnetocrystalline anisotropy (κ), and their saturation magnetization (M_s).[15] The saturation magnetization, M_s, is the magnetic moment of elementary atoms per unit weight where all of the dipoles are aligned parallel while in the magnetic field. When magnetic nanoparticles are placed in a saturating ac magnetic field, the magnetic moments align in the direction of the magnetic field. When the frequency of the ac magnetic field is high enough, there is a lag time that generates magnetic work (W). This magnetic work is stored as internal energy (U). Because thermodynamically, $dU = \delta Q + \delta W$, the internal energy will be converted into heat dissipation (Q).[14−17] Heat generation in the magnetic nanoparticles in a fluidic medium is the summation of (1) relaxation processes, including Néel and Brownian relaxations, (2) hysteresis, and (3) viscous forces.[14−17] The heat generation in the solid state, such as magnetic polymer nanocomposites, arises only from the Néel relaxation and the hysteresis where Brownian relaxations and viscous friction dissipations are absent.

Structural polymer and polymer composite materials are constantly under static and cyclic loads, which results in micro cracks, defects, and failure over time. In addition, homolytic and heterolytic chain scissions occur due to exposure to UV, ozone, heat, or aging. Reversible urethane, urea, and Diels–Alder chemistries can also result in chain scission. The micro cracks adversely affect thermal, mechanical, electrical, and durability performance of advanced structural materials. Smart bioinspired methods of polymer self-healing are highly desirable to repair these microcracks and other damage and defects in polymeric materials.[18−21] Chemical methods of self-healing using a tube

Received: November 26, 2014
Accepted: July 20, 2015
Published: July 20, 2015

© 2015 American Chemical Society

DOI: 10.1021/acsami.5b04314
ACS Appl. Mater. Interfaces 2015, 7, 16932−16937

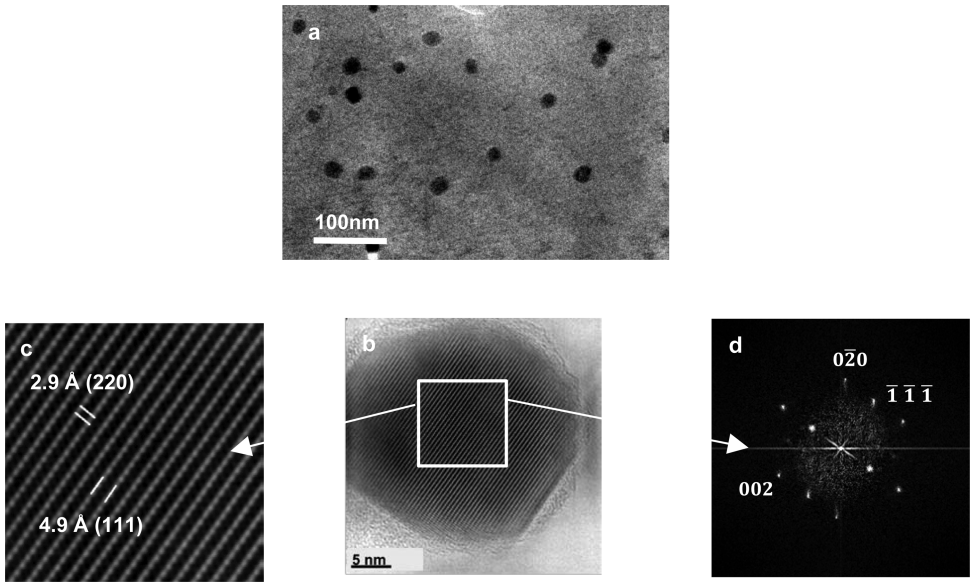

Figure 1. (a) Iron cobalt oxide iron manganese oxide core−shell nanoparticles. (b) High-resolution micrograph of the core−shell magnetic nanoparticles. (c) High-resolution micrograph of lattice fringes of the iron manganese shell. (d) The Fourier transform of the iron manganese oxide lattice fringes.

or microballoon-encapsulated active monomer dispersed in a polymer containing catalyst or activator have been studied.[18−21] During crack initiation, microballoons rupture and result in a reaction of the monomer and the polymer in the presence of a catalyst. Diels−Alder chemistry using furan and maleimide-based compounds have been widely studied.[18−21] Incorporation of microballoons containing conductive carbon powder, metallic microwires, and healing agents reports the crack location through electrical conductivity.[22] Sulfide and disulfide chemistry have also been used as a basis for self-healing polymer systems.[23,24] Meanwhile, the majority of reported self-healing research has been focused on micron-sized healing of cracks;[18−24] however, a more recent work reports a novel two-step method based on formation of acrylic fast gel with controlled slow kinetics which cross-links and permits larger millimeter size area restoration in large structural components.[25]

Here, we report the use of magnetic polystyrene nanocomposites in a high-frequency ac magnetic field as a novel, repeatable, and controllable method of self-healing. This idea is based on the heat generation of magnetic nanoparticles when placed in an ac magnetic field. The heat generation contributes to physical and chemical changes in the polymer matrix resulting in healing and restoration of damage. Biomedical research on hyperthermia has examined heat generation by magnetic nanoparticles in a fluidic medium as a means of treating certain cancers.[11−15] The thermal energy generated in magnetic nanoparticle suspension systems is due to viscous frictions, hysteresis, and Néel and Brownian relaxations.[15−17] We demonstrate that in the absence of viscous frictions and Brownian relaxations in the solid state, it is possible to generate heat only due to hysteresis and Néel relaxation. The thermal energy generated by magnetic nanoparticles in the ac magnetic field results in mesoscale and macroscale physical changes in the polymer matrix and leads in healing of the cracks in the polymer. Through optimization of magnetic properties for magnetic polystyrene nanocomposites and the applied ac magnetic field parameters, a high heat generation was achieved. The high heat generation resulted in fusing and melting in the defected large area, which leads to restoration and healing. Magnetization of the magnetic polystyrene nanocomposites can be tuned to achieve specific targeted temperature. Magnetic polystyrene nanocomposites can be melted in ac magnetic field at 230 °C in the solid state with 3.5 wt % magnetic nanoparticles to heal large area defects. The highest temperature of 320 °C was obtained with 10 wt % magnetic nanoparticles which was below the onset of PS degradation. This study is significant in the use of high performance polymers and polymer composites in advanced technology applications. High-performance polymers have high glass transition temperature and high thermal stability. These types of polymers require high heat generation to induce physical changes. In addition, heat generated by magnetic nanocomposites can be studied to design thermoset polymers that thermally induce both physical and chemical changes in the polymer matrix. The nanocomposite developed in this study showed an unprecedented high level of controllable thermal energy generation that can be used not only in the reported polystyrene but also for a range of high-temperature polymers with high glass transition temperatures.

2. RESULTS AND DISCUSSION

2.1. Core−Shell Magnetic Nanoparticles. Core−shell magnetic nanoparticles with an iron cobalt oxide core and iron manganese shell were synthesized using a modified published protocol (Supporting Information).[15] In liquid dispersions used for hyperthermia, these core−shell magnetic nanoparticles have demonstrated high heat generation due to exchange coupling.[15] The present study relies on the same theory of high heat generation by magnetic nanoparticles over a range of optimized parameters in an ac magnetic field but in the solid-state polystyrene nanocomposite. The magnetic nanoparticles have an organic layer corona on the surface which makes them compatible with the polystyrene polymer matrix.

The magnetic nanoparticle structure was investigated by high-resolution transmission electron microscopy (HR-TEM). High-resolution electron microscopy is essential to investigate

DOI: 10.1021/acsami.5b04314
ACS Appl. Mater. Interfaces 2015, 7, 16932−16937

the morphology of nanoparticles in the polymer nanocomposites.[26,27] The first step of the synthesis reaction resulted in an iron cobalt oxide (Fe_2CoO_4) core. Addition of the Fe_2MnO_4 shell to the Fe_2CoO_4 core resulted in magnetic nanoparticles with an average diameter of 19.49 ± 3.9 nm (Figure 1a–c). The high-resolution TEM micrograph shows the lattice crystalline structure of the Fe_2MnO_4 with a 220 lattice structure of ~2.97 Å (Figure 1b,c). Figure 1d shows the fast Fourier transform of Figure 1b, demonstrating the diffraction pattern of the Fe_2MnO_4. Magnetic nanoparticles exhibit aggregation and agglomeration due to both van der Waal forces and attractive magnetic coercive forces. The HR-TEM micrograph shown in Figure 1b shows interplanar distances of 0.29 and 0.49 nm, which corresponds to the {220} and {111} planes of a $MnFe_2O_4$ crystalline cubic structure. The fast Fourier transform (FFT) analysis in Figure 1d shows the particle's diffraction pattern with orientation in the [100] direction.

Thermal gravimetric analysis (TGA) was performed to determine the organic content of the iron cobalt oxide (Fe_2CoO_4) iron manganese oxide (Fe_2MnO_4) core–shell nanoparticles (Figure 2a). The sample initially had a steady

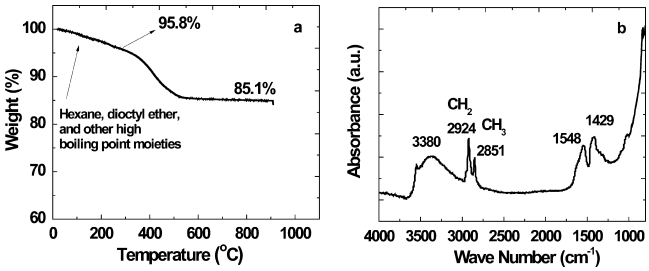

Figure 2. (a) Thermal gravimetric data of the iron cobalt oxide (Fe_2CoO_4) iron manganese oxide (Fe_2MnO_4) core–shell nanoparticles showing 10.7% organic content. (b) FT-IR spectra of organic corona present on the surface of core–shell magnetic nanoparticles.

weight loss that was due to the removal of residual small molecules and solvents. Hexane (bp: 68 °C) and dioctyl ether (bp: 287 °C) were the reaction solvents, where the TGA curve shows 95.8% weight loss. There is negligible weight loss at temperatures higher than 287 °C below the onset of organic layer degradations, which could be due to the higher boiling point amine and other moieties. Decomposition of organic layer starts at 370 °C, and the sample reaches a final weight of 85.1%. Thus, the nanoparticle organic surface coating is approximately 10.7 wt %. An organic content value of 10.7% ± 0.6% is an average of several TGA runs of multiple batches. FT-IR was used to characterize the organic surface moieties on the core–shell magnetic nanoparticles (Figure 2b). Absorption peaks at 2851 and 2924 cm^{-1} are C–H stretch, and 1429 is C–H bending of CH_3 and CH_2 in linear alkyl chain. The peak at 1548 cm^{-1} could be due to the N–H stretch of the trace amount of the alky amine precursors (oleyl amine and trioctyl amine) on the nanoparticle surface. The peak at 3380 cm^{-1} could be due to the stretch of the O–H group or N–H group. The hydroxyl group could be present on the surface of the Fe_2MnO_4.[28]

Magnetic characteristics of the nanoparticles were studied using an ac field gradient magnetometer. Figure 3 shows the mass normalized hysteresis loop for the iron cobalt oxide (Fe_2CoO_4) iron manganese oxide (Fe_2MnO_4) magnetic core–

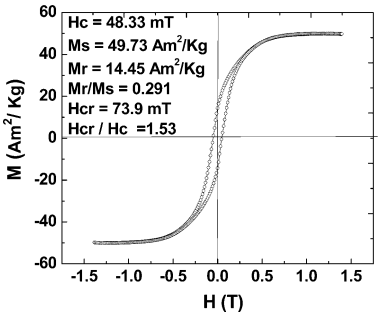

Figure 3. Hysteresis plot of magnetic moment vs magnetic field for iron cobalt oxide core with the iron manganese oxide shell.

shell nanoparticles. The magnetic saturation (M_s) and saturation remanent magnetization (M_r) were 49.7 Am^2/kg, and 14.5 Am^2/kg, respectively. The coercive force (H_c) was 48.3 mT. Our previously synthesized iron manganese oxide (average diameter 6.11 ± 0.69 nm) had M_s, M_r, and H_c of 33.73 Am^2/kg 125.1 mAm^2/kg, and H_c of 0.593 mT.[6] The size of iron cobalt oxide core manganese oxide shell nanoparticles were larger (19.49 ± 3.9 nm), exceeding the critical diameter of iron manganese oxide (9 nm) and iron cobalt oxide. The coercive force, H_c shows an increase from 0.593 mT to 48.3 mT due to the iron cobalt magnetic core and a size exceeding critical superparamagnetic limit. The magnetization loop of core–shell nanoparticles in Figure 3 shows hysteresis and loop. This indicated a size exceeding the superparamagnetic critical diameter, where the nanoparticles are in the single domain regime. The ratio of M_r/M_s = 0.291 and H_{cr}/H_c = 1.53 might suggest that the magnetic nanoparticles have not reached multidomain and the magnetic moments are in the single domain regime. These nanoparticles with higher saturation magnetization and slight hysteresis were designed for higher heat generation when subjected to an ac magnetic field.

2.2. Magnetic Nanocomposites. Polystyrene nanocomposites were prepared with surface modified, core–shell magnetic nanoparticles at loading levels of 3.5, 10, and 20 wt %. The nanocomposites exhibited magnetic characteristics in a magnetic field. Table 1 shows averaged magnetic properties

Table 1. Magnetic Properties of Core–Shell Magnetic Nanoparticle Polystyrene Nanocomposites

magnetic polystyrene nanocomposite, magnetic wt %	H_c, mT	M_s, Am^2/kg	M_r, Am^2/kg
3.5	61.34	2.29	0.6
10	60.61	8.43	2.38
20	59.84	11.1	3.12

including H_c, coercivity, M_s, saturation magnetization, and M_r, remanent magnetization. All magnetic polystyrene nanocomposites show almost constant coercivity of 60.6 mT. The saturation magnetization, M_s, values for the 3.5, 10, and 20 wt % magnetic PS nanocomposites were 2.29, 8.43, and 11.1 Am^2/kg, respectively. Their saturation magnetization increased with increasing magnetic nanoparticle content. The remanent magnetization, M_r, also showed an increase with increasing magnetic nanoparticle content from 0.6 to 2.38 and 3.12 Am^2/kg for 3.5, 10, and 20 wt % magnetic PS nanocomposites.

All magnetic core–shell polystyrene nanocomposites exhibited a slight hysteresis loop similar to the individual nanoparticles. Figure 4 shows the hysteresis loop of the 10

DOI: 10.1021/acsami.5b04314
ACS Appl. Mater. Interfaces 2015, 7, 16932–16937

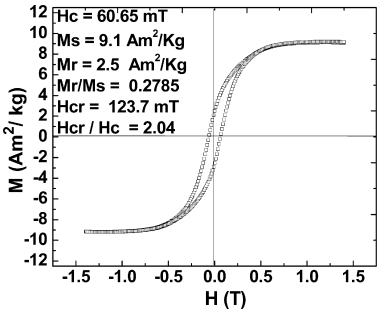

Figure 4. Hysteresis plot of magnetic moment vs magnetic field for 10 wt % iron cobalt oxide (Fe_2CoO_4) iron manganese oxide (Fe_2MnO_4) nanoparticle polystyrene nanocomposite.

wt % core−shell magnetic nanoparticle polystyrene nanocomposite sample. The presence of an open hysteresis loop indicates that the magnetic nanoparticles are above the critical diameter and larger than the superparamagnetic regime.

2.3. Heat Generation in ac Magnetic Field. Thermal energy storage depends upon the nanoparticle's magnetic characteristics, the time constants of the magnetic nanoparticles for Brownian relaxation and Néel relaxations, viscous dissipation, and hysteresis. Brownian relaxation can only generate heat when the particles can rotate freely in a fluidic medium. Néel relaxation is due to the internal fluctuation of magnetic moments within the crystal. The Néel relaxation time, τ_N, is given by eq 1 and is attributed to the anisotropic energy to the thermal energy. In eq 1, V is the particle volume, $\tau_0 = 10^{-9}$ s, κ is anisotropy constant, $K = 1.3806488 \times 10^{-23}$ m^2 kg s^{-2} K^{-1} is Boltzmann constant, and T is the temperature. The power dissipation, P, is given by eq 2 where μ_0 is a constant, f is the frequency, χ_0 is the susceptibility, and H_0 is the magnetic field.[12−15]

$$\tau_N = \tau_0 \exp[KV/(kT)] \quad (1)$$

$$P = \pi \mu_0 \chi_0 H_0^2 f \frac{2\pi f\tau}{1 + (2\pi f\tau)^2} \quad (2)$$

In order to increase power dissipation, P, high frequency and high magnetic field are required. Also, the magnetic characteristics, susceptibility (χ_0), and parameters that determine the time constant, τ, should be optimized to achieve high power dissipation values. Susceptibility is directly proportional to the saturation magnetization, $\chi_0 = \mu_0 M_s^2 V/(kT)$. Power dissipation is proportional to the specific loss power (SLP) using the average density.[14,15] It should be noted that eqs 1 and 2 provide only correlations between the magnetic properties (susceptibility, time constants, etc.), magnetic field, frequency of ac field, and the power dissipation.

A series of Fe_2CoO_4- Fe_2MnO_4 core−shell polystyrene nanocomposites were prepared and placed in an ac magnetic field. The ac magnetic field was optimized for these particular nanocomposites (5 kW @ 95% power, $f = 240 \pm 3$ kHz, coil 6 turn 1 in. diameter) (Figure 5). According to eqs 1 and 2, a high frequency is necessary to generate internal energy that could be converted to a high thermal energy. An IR pyrometer with a recording capability was used to record the surface temperature of the magnetic polymer nanocomposites while in the coil. The sample surface was not insulated, and therefore, free convection thermal transfer at the magnetic polystyrene nanocomposites surface exists. The magnetic polymer nanocomposites were placed in the optimized coil until they reached a temperature maximum and showed crack healing or ultimately melting. A control sample of neat polystyrene was placed in the inductive coil under the exact same magnetic field, and it did not exhibit any temperature change.

Polystyrene is a thermoplastic brittle polymer with a softening temperature of 95 °C, glass transition temperature of ∼100 °C, and a melting point in the range of 240−270 °C depending on its tacticity and crystallinity. Polystyrene starts to flow above its glass transition temperature at ∼115 °C. The onset of thermal degradation in air has been reported as ∼340 °C, where the polystyrene nanocomposites have much higher thermal stability.[29,30]

The maximum temperature on the core−shell magnetic PS nanocomposite surface increased with increasing magnetic nanoparticle content. The maximum surface temperatures were 230 and 320 °C for the 3.5 and 10 wt % nanocomposites, respectively (Figure 6). Core−shell magnetic polystyrene nanocomposite with a macrocrack was melted and exhibited melt flow in the magnetic field, making it possible to heal the crack forming a uniform area while the polystyrene was experiencing high temperature in the ac magnetic field. Figure 6 shows the change of temperature with time on the surface of 10 wt % magnetic polystyrene nanocomposite in the ac magnetic field. The maximum temperature reached 320 °C resulting in

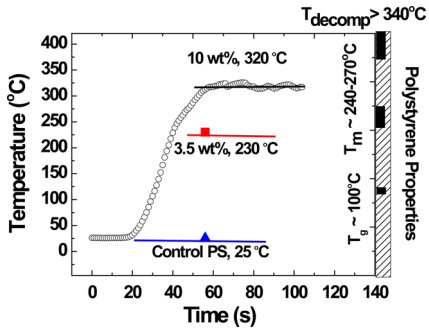

Figure 6. Surface temperature of 10 wt % magnetic polystyrene nanocomposite in ac magnetic field (○), temperature of 3.5 wt % magnetic polystyrene nanocomposite, red (■), and control PS temperature @ 25 °C, blue (▲).

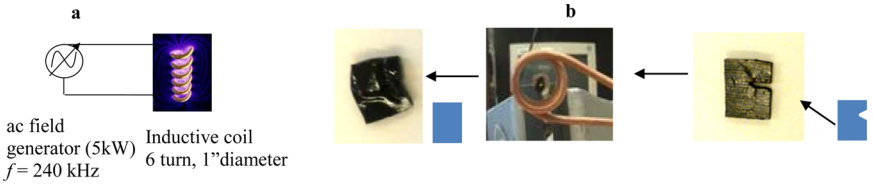

Figure 5. (a) Schematics of inductive heating using an ac magnetic field. (b) A piece of core−shell magnetic polystyrene nanocomposites (10 wt%) with macrocrack was placed in the ac magnetic coil (5 kW@95%, 240 kHz) and subsequently healed and melted together.

DOI: 10.1021/acsami.5b04314
ACS Appl. Mater. Interfaces 2015, 7, 16932−16937

full melting of the polystyrene. The 10 wt % magnetic polystyrene nanocomposites was removed from the field after 100 s to avoid possible onset of degradation.

The internal energy which is converted to the thermal energy results only from the Néel relaxation and hysteresis (solid state) for the magnetic polystyrene nanocomposites. The power dissipation eq 2 is proportional to the relaxation time, frequency, and susceptibility. The saturation magnetization of magnetic polystyrene nanocomposites increases with increasing magnetic nanoparticle content. Therefore, the higher concentration of magnetic nanoparticles likely leads to higher contributions of Néel relaxation resulting in higher heat generation. The magnetic characteristics of the nanoparticles, magnetic content and characteristics of the polystyrene nanocomposites, as well as magnetic field frequency and power can be optimized and tuned to obtain target temperature. High heat generation and temperatures are necessary for high-performance high-temperature polymers. The target temperature can be optimized to exceed the glass transition temperature surpassing chain segmental motion and providing enough energy for the polymer molecules to flow.

CONCLUSIONS

A series of iron cobalt oxide/iron manganese oxide core−shell magnetic nanoparticles were synthesized and incorporated into polystyrene via a solution precipitation method to generate magnetic polymer nanocomposites. The core−shell magnetic nanoparticles have high coercivity, saturation magnetization, and a slight hysteresis, suggesting domain states above the superparamagnetic boundary. When the magnetic polymer nanocomposites were placed in an ac magnetic field (high frequency and high power), they exhibited high heat generation due to Néel relaxation and hysteresis. The heat generation resulted in fusing and healing of large-scale cracks. The maximum heat generated (320 °C) on the nanocomposite's surface resulted in melting the polystyrene. This study presents a novel method of a self-healing polymer nanocomposites that is applicable to a high-performance polymers which require higher temperature for physical changes to occur.

ASSOCIATED CONTENT

Supporting Information

The Supporting Information is available free of charge on the ACS Publications website at DOI: 10.1021/acsami.5b04314.

Materials, synthesis methods of core−shell particles, and X-ray diffraction patterns of core and core−shell nanoparticles (PDF)

AUTHOR INFORMATION

Corresponding Author

*E-mail: mitra.yoonessi@gmail.com.

Notes

The authors declare no competing financial interest.

ACKNOWLEDGMENTS

The NASA Center Innovation Fund program and Structure and Materials Division are thanked for funding this project. Subsonics Fixed Wing Project, Fundamental Aeronautics Program (NASA Contract NNC07BA13B), NASA Center Innovation Fund Program, and Dr. Roshanak Hakimzadeh are thanked for funding and support of this research. Daniel A. Scheiman is thanked for the laboratory support.

REFERENCES

(1) Munaweera, I.; Aliev, A.; Balkus, K. J., Jr. Electrospun Cellulose Acetate-Garnet Nanocomposite MagneticFibers for Bioseparations. *ACS Appl. Mater. Interfaces* **2014**, *6*, 244−251.

(2) Fragouli, D.; Torre, B.; Villafiorita-Monteleone, F.; Kostopoulou, A.; Nanni, G.; Falqui, A.; Casu, A.; Lappas, A.; Cingolani, R.; Athanassiou, A. Nanocomposite Pattern-Mediated Magnetic Interactions for Localized Deposition of Nanomaterials. *ACS Appl. Mater. Interfaces* **2013**, *5*, 7253−7257.

(3) Li, S.; Lin, M. M.; Toprak, M. S.; Kim, D. K.; Muhammed, M. Nanocomposites of Polymer and Inorganic Nanoparticles for Optical and Magnetic Applications. *Nano Rev.* **2010**, *1*, 5214.

(4) Raj, P. M.; Sharma, H.; Reddy, G. P.; Altunyurt, N.; Swaminathan, M.; Tummala, R.; Nair, V. Cobalt-polymer Nanocomposite Dielectrics for Miniaturized Antennas. *J. Electron. Mater.* **2014**, *43*, 1097−1106.

(5) Mohr, R.; Kratz, K.; Weigel, T.; Lucka-Gabor, M.; Moneke, M.; Lendlein, A. Initiation of Shape-memory Effect by Inductive Heating of Magnetic Nanoparticles in Thermoplastic Polymers. *Proc. Natl. Acad. Sci. U. S. A.* **2006**, *103*, 3540−3545.

(6) Yoonessi, M.; Peck, J. A.; Bail, J. L.; Rogers, R. B.; Lerch, B. A.; Meador, M. A. Transparent Large-Strain Thermoplastic Polyurethane Magnetoactive Nanocomposites. *ACS Appl. Mater. Interfaces* **2011**, *3*, 2686−2693.

(7) Gass, J.; Poddar, P.; Almand, J.; Srinath, S.; Srikanth, H. Superparamagnetic Polymer Nanocomposites with Uniform Fe_3O_4 Nanoparticle Dispersions. *Adv. Funct. Mater.* **2006**, *16*, 71−75.

(8) Wilson, J. L.; Poddar, P.; Frey, N. A.; Srikanth, H.; Mohomed, K.; Harmon, J. P.; Kotha, S.; Wachsmuth, J. Synthesis and Magnetic Properties of Polymer Nanocomposites with Embedded Iron Nanoparticles. *J. Appl. Phys.* **2004**, *95*, 1439.

(9) Ohlan, A.; Singh, K.; Chandra, A.; Dhawan, S. K. Microwave Absorption Properties of Conducting Polymer Composite with Barium Ferrite Nanoparticles in 12.4−18 GHz. *Appl. Phys. Lett.* **2008**, *93*, 053114−053114.

(10) Lu, A.-H.; Salabas, E. L.; Schuth, F. Magnetic Nanoparticles: Synthesis, Protection, Functionalization, and Application. *Angew. Chem., Int. Ed.* **2007**, *46*, 1222−1244.

(11) Sun, S.; Murray, C. B.; Weller, D.; Folks, L.; Moser, A. Monodisperse FePt Nanoparticles and Ferromagnetic FePt Nanocrystal Superlattices. *Science* **2000**, *287*, 1989−1992.

(12) Lee, J.-H.; Huh, Y.-M.; Jun, Y.-w.; Seo, J.-w.; Jang, J.-t.; Song, H.-T.; Kim, S.; Cho, E.-J.; Yoon, H.-G.; Suh, J.-S.; Cheon, J. Artificially Engineered Magnetic Nanoparticles for Ultra-Sensitive Molecular Imaging. *Nat. Med.* **2007**, *13*, 95−99.

(13) Jang, J.-t.; Nah, H.; Lee, J.-H.; Moon, S. H.; Kim, M. G.; Cheon, J. Critical Enhancements of MRI Contrast and Hyperthermic Effects by Dopant-Controlled Magnetic Nanoparticles. *Angew. Chem., Int. Ed.* **2009**, *48*, 1234−1238.

(14) Veiseh, O.; Gunn, J.; Zhang, M. Design and Fabrication of Magnetic Nanoparticles for Targeted Drug Delivery and Imaging. *Adv. Drug Delivery Rev.* **2010**, *62*, 284−304.

(15) Lee, J.-H.; Jang, J.-t.; Choi, J.-s.; Moon, S. H.; Noh, S.-h.; Kim, J.-w.; Kim, J.-G.; Kim, I.-S.; Park, K. I.; Cheon, J. Exchange-Coupled Magnetic Nanoparticles for Efficient Heat Induction. *Nat. Nanotechnol.* **2011**, *6*, 418−422.

(16) Hergt, R.; Dutz, S.; M̈uller, R.; Zeisberger, M. Magnetic Particle Hyperthermia: Nanoparticle Magnetism and Materials Development for Cancer Therapy. *J. Phys.: Condens. Matter* **2006**, *18*, S2919−S2934.

(17) Rosensweig, R. E. Heating Magnetic Fuid with Alternating Magnetic Field. *J. Magn. Magn. Mater.* **2002**, *252*, 370−374.

(18) Ye, X. J.; Zhang, J.-L.; Zhu, Y.; Rong, M. Z.; Zhang, M. Q.; Song, Y. X.; Zhang, H. X. Ultrafast Self-Healing of Polymer toward Strength Restoration. *ACS Appl. Mater. Interfaces* **2014**, *6*, 3661−3670.

(19) Pratama, P. A.; Sharifi, M.; Peterson, A. M.; Palmese, G. R. Room Temperature Self-Healing Thermoset Based on the Diels−Alder Reaction. *ACS Appl. Mater. Interfaces* **2013**, *5*, 12425−12431.

DOI: 10.1021/acsami.5b04314
ACS Appl. Mater. Interfaces 2015, 7, 16932−16937

(20) Stukalin, E. B.; Cai, L.-H.; Kumar, N. A.; Leibler, L.; Rubinstein, M. Self-Healing of Unentangled Polymer Networks with Reversible Bonds. *Macromolecules* **2013**, *46*, 7525−7541.
(21) Fickert, J.; Makowski, M.; Kappl, M.; Landfester, K.; Crespy, D. Efficient Encapsulation of Self-Healing Agents in Polymer Nanocontainers Functionalized by Orthogonal Reactions. *Macromolecules* **2012**, *45*, 6324−6332.
(22) Hong, Y.; Su, M. Multifunctional Self-Healing and Self-Reporting Polymer Composite with Integrated Conductive Microwire Networks. *ACS Appl. Mater. Interfaces* **2012**, *4*, 3759−3764.
(23) Lafont, U.; van Zeijl, H.; van der Zwaag, S. Influence of Cross-linkers on the Cohesive and Adhesive Self-Healing Ability of Polysulfide-Based Thermosets. *ACS Appl. Mater. Interfaces* **2012**, *4*, 6280−6288.
(24) Canadell, J.; Goossens, H.; Klumperman, B. Self-Healing Materials Based on Disulfide Links. *Macromolecules* **2011**, *44*, 2536−2541.
(25) White, S. R.; Moore, J. S.; Sottos, N. R.; Krull, B. P.; Santa Cruz, W. A.; Gergely, R. C. R. Restoration of Large Damage Volumes in Polymers. *Science* **2014**, *344*, 620−623.
(26) Solá, F.; Xia, Z.; Lebrón-Colón, M.; Meador, M. A. Transmission Electron Microscopy of Single Wall Carbón Nanotube/Polymer Nanocomposites: A first-principles Study. *Phys. Status Solidi RRL* **2012**, *6*, 349−351.
(27) Solá, F.; *SEM and TEM Characterization of Polymer CNT Nanocomposites, in Polymer Nanotube Nanocomposites: Synthesis, Properties, and Applications*, 2nd ed.; Mittal, V., Ed.; John Wiley & Sons, Inc.: Hoboken, NJ, 2014; pp 167−185.
(28) Coates, J. Interpretation of Infrared Spectra. A Practical Approach. In *Encyclopedia of Analytical Chemistry*; Meyers, R. A., Ed.; John Wiley & Sons: Hoboken, NJ, 2000; pp 10815−10837.
(29) Fernandes, L.; Gaspar, H.; Bernardo, G. Inhibition of Thermal Degradation of Polystyrene by C60 and PCBM: A Comparative Study. *Polym. Test.* **2014**, *40*, 63−69.
(30) Blanco, I.; Abate, L.; Agatino Bottino, F.; Bottino, P. Thermal Degradation of Hepta Cyclopentyl, Mono Phenyl-polyhedral Oligomeric Silsesquioxane (hcp-POSS)/Polystyrene (PS) Nanocomposites. *Polym. Degrad. Stab.* **2012**, *97*, 849−855.

DOI: 10.1021/acsami.5b04314
ACS Appl. Mater. Interfaces 2015, 7, 16932−16937